Records of organically bound iodine during the Cenomanian–Turonian OAE 2: implications for bottom-water conditions and iodine sink

Xiaoli Zhou[a,b], Hugh C. Jenkyns[c], Wanyi Lu[a], Dalton S. Hardisty[d], Jeremy D. Owens[e], Timothy W. Lyons[f] and Zunli Lu[a*]

a Department of Earth Sciences, Syracuse University, Syracuse, NY

b Department of Marine and Coastal Sciences, Rutgers University, New Brunswick, NJ

c Department of Earth Sciences, University of Oxford, Oxford, UK

d Department of Geology and Geophysics, Woods Hole Oceanographic Institution, Woods Hole, MA

e Department of Earth, Ocean and Atmospheric Science, Florida State University, Tallahassee, FL

f Department of Earth Sciences, University of California, Riverside, CA

*Email: zunlilu@syr.edu

Key words: I/TOC, bottom water, OAE 2, black shale, Baltic

Abstract:

Oceanic Anoxic Events (OAEs) are characterized by deposition of widespread organic-rich marine sediments (black shales) and represent major disturbances to the global carbon cycle. Carbonate-associated iodine (I/Ca) has been used to indicate local, upper-ocean redox conditions, demonstrating highly dynamic spatial and temporal patterns at multiple sections during the Cenomanian–Turonian OAE 2 at ~94 Ma (Late Cretaceous). To further explore the utility of

iodine as a paleo-environmental proxy, we describe a new method of extracting organically bound iodine (I_{org}) from shale using volumes of samples on the order of tens of milligrams, offering the potential for high-resolution work across thin shale bands. The ratio of I_{org} to total organic carbon (I/TOC) in modern surface and subsurface sediment decreases with decreasing bottom-water oxygen, suggesting that iodine burial may have been influenced by redox changes. We evaluate I/TOC proxy in Holocene sediments from the Baltic Sea, Landsort Deep (IODP 347) and discuss those data within a framework of independent redox proxies. The results imply that I/TOC may be sensitive to hypoxic conditions, complementary to other anoxic–euxinic proxies. For OAE 2, we generated I/TOC and I_{org} records from six sections: Tarfaya (Morocco), Furlo (central Italy), Demerara Rise (western equatorial Atlantic), Cape Verde Basin (eastern equatorial Atlantic), South Ferriby (UK), and Kerguelen Plateau (southern Indian Ocean), which provides a broad spatial coverage to test the proxy. Generally, I/TOC decreases over the interval recorded by the positive carbon isotope excursion, the hallmark of OAE 2, suggesting an expansion of more reducing bottom-water conditions, consistent with independent constraints from iron speciation and redox-sensitive trace-metals (e.g., Mo). Relatively higher I/TOC values (thus more oxic conditions) are recorded in two OAE 2 high-latitude sites, supporting model simulations from previous works indicating higher bottom water oxygen concentrations in these regions.

1. Introduction

1.1. OAE 2 and redox proxies

Oceanic Anoxic Events (OAEs) are characterized by globally distributed marine deposition of organic-rich sediments known colloquially as black shales (Schlanger and Jenkyns,

1976; Jenkyns, 1980; Arthur et al., 1990; Jones and Jenkyns, 2001; Jenkyns, 2010). Black shales typically result from the combination of increased primary productivity coupled with enhanced preservation of organic matter in oxygen-depleted environments (e.g., Demaison and Moore, 1980; Schlanger et al., 1987; Arthur et al., 1988). The enhanced global burial of isotopically light organic-carbon in terrestrial and marine reservoirs can be fingerprinted through a positive carbon isotope excursion (CIE) spanning this event. (Tsikos et al., 2004; Hasegawa, 1997; Barclay et al., 2010; Jarvis et al., 2011).

OAE 2 and other OAEs have been linked to the eruption of large igneous provinces (LIPs), which released CO_2 to the atmosphere, increasing atmospheric temperature and strengthening hydrological cycling (e.g., Kerr, 1998; Jenkyns, 2003; Kuroda et al., 2007; Turgeon and Creaser, 2008; Adams et al., 2010). As a result, weathering rates of continents and exposed oceanic crust increased (Blattler et al., 2011; Pogge von Strandmann et al., 2013; Jenkyns et al., 2017), which delivered more nutrients to the oceans and stimulated marine productivity. Enhanced productivity resulted in a positive feedback that shuttled more organic matter to the greater depth, which in turn consumed more dissolved oxygen and induced oceanic deoxygenation in many regions—further favoring widespread burial of organic carbon (Jenkyns, 2003, 2010; Adams et al., 2010; Owens et al., 2016).

A wide range of proxies have been used to track water-column redox conditions. Biotic proxies such as foraminiferal assemblages have been used as indicators for dissolved oxygen levels (Friedrich et al., 2006; Takashima et al., 2009; Gertsch et al., 2010; El-Sabbagh et al., 2011; Bomou et al., 2013; Reolid et al., 2015). Trace-metal enrichment and Fe-speciation data from bulk shale have proven to be powerful tools to characterize redox changes during OAE 2 (van Helmond et al., 2014; Westermann et al., 2014; Junium et al., 2015; Poulton et al., 2015;

Jenkyns et al., 2017; Owens et al., 2016) and specifically allow us to track the presence or absence of euxinia during this event (Algeo and Lyons, 2006; Algeo and Tribovillard, 2009; Poulton and Canfield, 2005, 2011). Biomarkers (e.g., isorenieratane) indicate euxinia in the photic zone in proto-North and South Atlantic Ocean during OAE 2 (Sinninghe Damsté and Koster, 1998; Kuypers et al., 2002; Pancost et al., 2004; Hetzel et al., 2011).

Carbonate I/Ca is a relatively new proxy for redox reconstructions in the upper ocean and is very sensitive to the transition between oxic and suboxic conditions (Lu et al., 2010; Zhou et al., 2015; Lu et al., 2016; Owens et al., 2017). However, a major portion of sedimentary iodine is found within organic matter (Muramatsu and Wedepohl, 1998), and in this study, we test the potential of the ratio of organically bound iodine to total organic-carbon (I/TOC) as a proxy for bottom-water oxygenation. We then apply that proxy to six sections spanning OAE 2 and find evidence for expanded oxygen deficiency in bottom waters during the event, possibly even at high latitudes.

1.2. Organically bound iodine in recent sediments

The iodine concentration in modern seawater is relatively uniform around 0.45 μmol/l, with slightly higher amounts in the deep ocean (Elderfield and Truesdale, 1980). Iodate is the predominant iodine species in oxygenated seawater and is thermodynamically stable (Tsunogai, 1971; Wong, 1980). Iodate is slightly depleted in surface ocean waters, due to uptake by phytoplankton, and remains at constant concentration in a fully oxygenated water column (e.g., Bluhm et al., 2011). Iodine is taken up by marine plankton in the surface ocean at an average stoichiometry of 140 ± 80 μmol/mol to carbon (I/TOC) (Elderfield and Truesdale, 1980), although the reasons for and mechanisms behind this uptake in phytoplankton are not clear. The

93 presence of iodide (the reduced iodine species) in the surface ocean may be associated with
94 iodate reduction mistaken for nitrate by the enzyme nitrate reductase (Tsunogai and Sase, 1969).
95 Waite and Truesdale (2003) challenged this hypothesis, claiming that iodate reduction could be
96 independent of the presence or absence of nitrate reductase activity. Iodine concentrations in
97 exported particles may decrease when particulate materials sink through the water column (e.g.,
98 from 200–300 to 100–200 ppm, Brewer et al., 1980).
99 At the seafloor, I/TOC values of surface sediments depend on the bottom water
100 oxygenation condition. Iodine is enriched in the organic fraction (not in mineral phases) of
101 sediments deposited under well-oxygenated bottom water, yielding sediment I/TOC values
102 above 2000 μmol/mol (Fig. 1)(Price and Calvert, 1973; Kennedy and Elderfield, 1987b).
103 Locations with oxygen-depleted bottom waters have lower I/TOC (Price and Calvert, 1973), on
104 the same order of magnitude as the average I/TOC in plankton of 140 ± 80 μmol/mol (Elderfield
105 and Truesdale, 1980). I/TOC decreases rapidly from surface to subsurface sediments (< 1 m) at
106 oxygenated sites, whereas the ratios remain relatively stable at sites with low bottom-water
107 oxygen contents (Price and Calvert, 1977). Price and Calvert (1973) predicted that the
108 contrasting burial behavior of iodine in oxidizing versus reducing environments should be
109 recorded in ancient sediments.
110 The measurements of sedimentary iodine concentrations in these earlier investigations
111 (e.g., Price and Calvert, 1973) do not differentiate iodine associated with organic matter,
112 carbonate or residual porewater, although the signals were generally interpreted to be driven by
113 organic matter. For simplicity purpose, we refer to the total sedimentary iodine to organic carbon
114 ratio in the literature as I/TOC. Thus, the literature data compiled in Figure 1 serve as a
115 hypothesis instead of a quantitative calibration between oxygen and I/TOC. To better test this

hypothesis, (1) we develop a new method to extract iodine associated with organic matter, especially suitable for paleoenvironmental reconstruction work, (2) cross-examine the I/TOC proxy signal against other well-established proxies in Holocene sediments, (3) apply I/TOC in ancient sediments to obtain qualitatively records of local bottom-water redox conditions during OAE 2.

2. Study sites

As a proof of concept of the I/TOC proxy in recent sediments, we measured I/TOC ratios from a Holocene core of organic-rich, laminated sediments from a currently euxinic sub-basin of the Baltic Sea, Landsort Deep, from Site M0063 of IODP Expedition 347 (Andrén et al., 2015; Hardisty et al., 2016). We compare I/TOC data from Landsort Deep to previously published Mo concentrations and Fe speciation results from the same samples that indicate two past euxinic periods overlapping with intervals of enhanced organic carbon burial (TOC up to 8 wt. %) (Hardisty et al., 2016), providing both a multi-proxy comparison and paleoenvironmental context.

We studied the record of OAE 2 in six sections that capture different environmental settings (Fig. 2). Five out of six sites are in the proto-North Atlantic or close to the western Tethys, and one site is from the Southern Ocean. Although all of these sites contain layers of organic-rich sediments, local paleoenvironments vary, including different oceanographic settings, latitudes, water depths and behaviors of redox-sensitive trace elements. This sample collection provides a comprehensive framework for exploring iodine cycling during OAE 2.

A well-preserved sequence of glauconitic calcareous sandstone and organic-rich chalks was cored at Ocean Drilling Program (ODP) Site 1138 on the western margin of the central Kerguelen Plateau, a huge Early Cretaceous oceanic igneous plateau in the paleo-Indian Ocean

sector of the Southern Ocean at a modern water depth of 1141 m (Coffin et al., 2000; Holbourn and Kuhnt, 2002; Murphy and Thomas, 2012). The sediments from the Kerguelen Plateau studied here consist of black organic-rich claystones, virtually barren of calcareous foraminifera during OAE 2, although the overlying sediments contain moderately to well-preserved species (Holbourn and Kuhnt, 2002). We studied part of the black-shale interval, including the recovery stage of the CIE as expressed in the organic-carbon isotope data. The average TOC content at this section is 7.7%, intermediate among all the six studied sites, which range from 2.4% to 24.0%. $CaCO_3$ percentage remains close to zero for most of the carbon-isotope excursion (CIE) and recovers to ~40% at the end of the CIE, suggesting low production and/or low preservation of carbonate during the event (Fig. 6).

All other sites are in the pelagic proto-North and equatorial Atlantic Ocean and its continental margins. Deep Sea Drilling Project (DSDP) Site 367 is located in the Cape Verde Basin, 330 km west of the African coast, at a current water depth of 4748 m and a paleodepth of 3700 m (Lancelot et al., 1977; Chenet and Francheteau, 1979; Westermann et al., 2014). The studied cores consist of black, organic-rich shale interbedded with silty turbidites and TOC that ranges from 4% to 48% (Lancelot et al., 1977; Jones et al., 2007). Clay and organic debris are common, with rare pyrite and traces of bioturbation and rare to common foraminifera and nannofossils (Lancelot et al., 1977). Our study of this core covers the early stage of the CIE and several meters below. The maximum TOC value is the highest among the six studied sections (Fig. 6).

Tarfaya, in southwest Morocco, is a section of organic-rich, shallow marine sediments that span the Cenomanian-Turonian boundary (Kolonic et al., 2005). Core S57 (drilled by the Moroccan State Oil Company and Shell during exploration in the late 1970s and early 1980s:

Kolonic et al., 2005) records the deepest part of the basin with a reconstructed paleo-water depth of ~250–300 m. The core comprises ~37 m of organic-rich calcareous sediment containing planktonic foraminifera and nannofossils, with light- and dark-colored layers that alternate at a decimeter scale (Tsikos et al., 2004). TOC (wt. %) fluctuates between 0 and 15% for most of the section, with a peak value of 25% corresponding to the early stage of the CIE (Fig. 6). Other dominant sediment components in this section include carbonate, finely dispersed biogenic silica and clay (Leine, 1986; Tsikos et al., 2004).

The Furlo section of the pelagic Scaglia Bianca Formation was deposited at~20°N in western Tethys, central Italy (Lanci et al., 2010). The lower 17.5 m of section consists of rhythmically developed, light gray foraminiferal-nannofossil limestones, locally with pink, gray and black cherts—the latter associated with thin (sub-cm-scale) laminated black shales in parts of the section and TOC of up to ~20% (Turgeon and Brumsack, 2006; Jenkyns et al., 2007; Mort 2007a; Mitchell et al., 2008; Gambacorta et al., 2015). This limestone sequence is overlain by the Bonarelli Level, recording the impact of OAE 2, characterized by interbedded black laminated organic-rich shale (TOC 0.5–18%), gray claystone and brown radiolarian sand, with a total thickness of ~1 m (Fig. 6). A low-resolution organic $\delta^{13}C$ record shows a gradual rise from -26.5‰ to -25.5‰ in sediments below the Bonarelli Level, with values increasing abruptly to -23.5‰ at the onset of the positive CIE and fluctuating between -24 and -23 ‰ through the organic-rich unit (Jenkyns et al., 2007).

South Ferriby is located in Lincolnshire, northeast UK, and its sediments (English Chalk) were deposited on a shallow epicontinental pelagic shelf, adjacent to the proto-Atlantic Ocean. The section is comprised of relatively condensed organic-lean foraminiferal-nannofossil carbonates with TOC mostly between 1 and 2%, interrupted by a thin (~10 cm) layer of organic-

rich (max. TOC = ~8%) and laminated marls (Jenkyns et al., 2007; Pogge von Strandmann et al., 2013). The organic carbon-isotope profile gradually decreases upwards from -23 to -25 ‰ in the studied interval, capturing the upper part of the positive CIE (Fig. 6).

Site 1258 (ODP Leg 207) is situated on the northwest slope of Demerara Rise adjacent to Suriname and French Guyana in the western equatorial Atlantic Ocean, currently located at a water depth of 3192 m (Erbacher et al., 2004; Friedrich et al., 2006). The Cenomanian to Turonian sequence consists mainly of laminated, organic-rich, black shales with local occurrence of limestones, chert, phosphatic nodules and well-preserved fish debris (Hetzel et al., 2009). Clay content varies throughout the section, and the carbonate content is usually equal to or less than 50% in these organic-rich layers with TOC level of ~0.5-25% (Erbacher et al., 2004). The abundance of foraminifera varies drastically between lamina (Nederbragt et al., 2007).

3. Methods:

Various methods have been used to decompose and extract total iodine from sediment samples, such as dry ashing/alkaline fusion, microwave-assisted digestion and combustion (Knapp et al., 1998; Brown et al., 2005; Romarís-Hortas et al., 2009; Tinggi et al., 2011). The sample masses required for these methods are usually larger than 100 mg (e.g., Tullai et al., 1987; Knapp et al., 1998). Here we develop a new method for extracting organic iodine using much smaller samples of ~20 mg. Fine powders of sediment were weighed on a microbalance, decarbonated by adding 3% (v/v) nitric acid and then thoroughly rinsed with DI (deionized) water. The decarbonated samples were transferred into Teflon vials and mixed with 2 ml of tetramethylammonium hydroxide (TMAH 25% in H_2O, Sigma-Aldrich TraceSELECT®). The vials were tightly sealed and heated in the oven at 90 ℃ for 4–6 weeks. The sealed vials were

sonicated in a water bath for one hour daily. Approximately 20 μl of solutions were subsampled from each Teflon vial and diluted with DI water for preservation in a refrigerator. Sub-sampling was carried out 1–5 times a week during the entire heating period. Iodine concentrations were measured in the sub-sampled solutions to determine the time interval required to extract organic iodine from samples. Details of our method development are provided in the 'Results and discussion' section.

The bulk-rock samples from six OAE 2 sections were processed using the same method as described above, except that the sub-sampling was skipped and the heating time was shortened to 20 days, which we demonstrate to be sufficient to completely extract iodine from the samples (Fig. 3). Before iodine analysis by ICP-MS, the stored solutions were mixed with a freshly made matrix containing internal standards. Potassium iodide (KI, Alfa Aesar, 99.99% in purity) was dissolved and diluted to make calibration standards. The standard deviation for each measurement was mostly less than 1% and was always less than 5%. I/TOC values are reported as measured I_{org} concentration over the TOC content. I_{org} values are for bulk-rock weight of each sample.

4. Results and discussion

4.1. Method development

We selected two samples for a preliminary test of the extraction method, one from a pre-OAE interval, one from within the OAE interval, and a duplicate for each sample. A potassium iodide solution was set up as a control and processed with the same method as the OAE 2 samples. The iodine concentrations in subsampled solutions increased in the first 20 days and remained almost constant afterwards (Fig. 3a). This result suggests that 20 days is sufficient to

extract iodine from organic matter. The variation in KI concentrations (RSD = 5%) reflects the uncertainty in subsampling, preservation and measuring iodine on an ICP-MS but suggests that there was no major loss through volatilization during the experiment (Fig. 3a). The fluctuations in the KI control solutions were small, compared to the variability between OAE samples.

We also investigated the effect of sample mass on measured I/TOC values using the same two samples used for the preliminary test of the extraction method. Samples were weighed to ~5, 10, 20, 30, 40, and 50 mg and then treated following the same extraction method adopted for all the OAE 2 samples. The results suggest relatively constant I/TOC values with sample masses from 5 to 50 mg (Fig. 3b). Most of the data fall within the standard deviation of each set of I/TOC values, 6.6% and 5.1% for the pre-OAE and OAE samples respectively. All the OAE samples are abundant and thus we choose medium amount ~20 mg of well-homogenized powder for reconstructing stratigraphic trends. Samples as small as 5 mg appear to be sufficient for future high resolution work.

4.2. Hypothesis: I/TOC as a qualitative bottom-water oxygenation proxy?

We begin this discussion by exploring the I/TOC proxy in light of previous work. The positive correlation between I/TOC and bottom-water oxygenation in recent sediments (Price and Calvert, 1973) (Fig. 1) reveals the potential for the proxy to reconstruct palaeo-redox near the seafloor using ancient sediments. However, it is important to discuss fundamentals and limitations of I/TOC as an oxygenation indicator in terms of (i) the causes of the correlation between surface-sediment I/TOC and bottom-water oxygen level, (ii) preservation of the I/TOC gradient (and inferred oxygen gradient) among different sites in shallow subsurface sediments during early diagenesis and (iii) the influence of long-term burial.

The enrichment of iodine in oxic surface sediments (relative to marine plankton) has generally been interpreted to reflect organic-matter degradation and iodine recycling, but the detailed biogeochemical processes have not been clearly elucidated. Price and Calvert (1973) speculated that this enrichment is related to iodine sorption on the organic fraction, controlled by unspecified enzyme reactions at the surface of dead cells that occur only in an oxidizing environment. Francois (1987) specifically demonstrated a mechanism for iodine enrichment in surficial sediments under an oxic water column in which IO_3^- is reduced by humic substances and converted to iodinated organic molecules. Alternatively, in sediments underlying an oxic water column, sources of iodine in surficial sediments are suggested to be from the remineralization of organic matter just below the sediment-seawater interface, rather than from the bottom water (Kennedy and Elderfield, 1987b). Ullman and Aller (1985) introduced a hypothesis whereby IO_3^- is adsorbed to Fe-oxyhydroxides on the surface of oxic sediments. We postulate that the degree of iodine enrichment in surface sediment may be related to the concentrations of the oxidized iodine species (IO_3^-) in the bottom water. If that is the case, low I/TOC values can be interpreted as a signal for IO_3^- reduction in the bottom water, which occurs prior to iron and sulfate reduction (Rue et al., 1997), consistent with rapid decrease in I/TOC at 0–0.5 ml/l of [O_2] (Fig. 1). This relation between I/TOC and [O_2] indicates that the I/TOC proxy delineates hypoxic to anoxic settings, whereas Fe speciation and Mo concentrations has their advantages in anoxic to euxinic conditions. We aim to, preliminarily, test the reliability and redox window of I/TOC. Detailed biogeochemical mechanisms of iodine enrichment and remobilization in modern and ancient sediments are beyond the scope of this paper.

Significant decreases in I/TOC are observed just below the sediment-water interface in sediments beneath an oxic water column, with values steadily decreasing to near-constant values

278 within 0.5–2.5 meters below the sediment-water interface (Price et al., 1970; Price and Calvert,
279 1977). Under oxygenated bottom waters, I/TOC decreases rapidly in sediments, whereas low-
280 oxygen sites show a more stable I/TOC depth profile in shallow subsurface sediments (Price and
281 Calvert, 1977). However, higher I/TOC ratios seem to be preserved in subsurface sediments
282 under relatively well-oxygenated bottom waters compared to oxygen-depleted waters (Fig. 1).
283 Furthermore, sedimentation rates may impact the enrichment of iodine in surface sediment and
284 complicate I/TOC interpretions as bottom-water O_2 signature (Kennedy and Elderfield, 1987b).
285 Hence, the absolute values of subsurface I/TOC may be affected by non-redox-related factors.
286 Regardless, bottom-water O_2 gradients seem to act as an important control on the I/TOC gradient
287 among different sites. For these reasons, we do not recommend that specific I/TOC values from
288 modern surficial sediments be linked to a specific bottom-water O_2 concentration, but instead we
289 recommend evaluating relative changes in I/TOC at multiple sites as a qualitative tracer for the
290 presence of O_2 in the bottom water.
291 I/TOC data in ancient sediments cannot be directly compared with those in modern
292 sediments due to iodine loss during diagenetic alteration of organic matter. I/TOC values of the
293 OAE 2 samples are more than an order of magnitude lower than those in modern subsurface
294 sediments (Fig. 1), possibly indicating preferential release of iodine (relatively to carbon) during
295 the burial of organic matter over tens of millions of years. Nevertheless, there is potential for
296 preservation of the spatial and temporal patterns in bottom-water oxygen by I/TOC values in the
297 sediments deposited during OAEs and other ancient systems by analogy. OAE 2, characterized
298 by widespread deposition of organic-rich sediments, along with modern-recent sediments from
299 the Baltic, provides an ideal opportunity to test the fidelity of this new proxy. Given that the
300 hypoxic–anoxic redox window is where this proxy behaves with greatest sensitivity, as

documented in modern systems, I/TOC may be complementary to other proxies for bottom-water redox, such as Fe speciation, concentrations of redox-sensitive trace metals, better suited to more strongly reducing conditions.

4.3. Proxy validation in Holocene sediments from the Baltic Sea

The Landsort Deep is a modern anoxic basin with bottom water hydrogen sulfide accumulation (euxinia) and is among the most reducing sub-basins in the modern Baltic Sea. Holocene sediments are laminated and have large variations in TOC, Fe geochemistry (Fe_T/Al, Fe_T/Al, (Fe_{py}+Fe_{AVS})/Fe_{HR}) and Mo concentrations confined to distinct intervals (Fig. 4). Elevated Fe_T/Al and Fe_T/Al are diagnostic of anoxic water columns (Algeo and Lyons, 2006; Raiswell and Canfield, 1998), and when these Fe enrichments overlap with Mo enrichments of >25 and (Fe_{py}+Fe_{AVS})/Fe_{HR}) approaching 1, they are diagnostic of euxinic bottom waters (Poulton and Canfield, 2011; Algeo and Lyons, 2006). Previous work has shown that the two periods of elevated TOC at Landsort Deep overlap with large-scale Baltic anoxic events: the Medieval Warm Period (MCA; 1.250 to 0.8 ka) and the Holocene Thermal Maximum (HTM; ~8-4 ka) (Andren et al., 2011; Hardisty et al., 2016). The elevated Fe and Mo data from these same periods (Fig. 4) uniquely indicate euxinia at Landsort Deep, analogous to today (Hardisty et al., 2016; Noordman et al., 2016).

Most of the I/TOC values through the section are <100 μmol/mol (Fig. 4), falling into the hypoxic to suboxic range based on the compiled literature data in Figure 1. Importantly, I/TOC shows a pulsed increase in I/TOC (~2–3 m) during the interval between the two most recent euxinic periods overlapping with the Medieval Climate Anomaly (MCA) and modern sediments (Fig. 4). We emphasize that the pulse of high I/TOC is not within surficial sediments and is

unlikely a diagenetic artifact of decreasing sedimentary iodine following progressive organic matter remineralization (see previous section). The shallowest sample from this section is at 0.7 m with an I/TOC value of 102 μmol/mol, whereas increase in I/TOC was observed directly below this sample (Fig. 4). Rather than diagenetic overprints, this I/TOC pattern likely reflects a period with relatively oxygenated bottom waters compared to the surrounding euxinic periods in the Landsort Deep.

A cross-plot between I/TOC and trace metal proxies (Fig. 5) demonstrates that high I/TOC values are sensitive to the transition from hypoxic to anoxic condition, but there are no clear indications that the I/TOC proxy can separate anoxia from euxinia. That distinction is instead the purview of Fe speciation and Mo enrichment patterns. The combined Landsort Deep data (Figs. 4-5) highlight the fact that the I/TOC value does not increase during periods independently inferred to be euxinic. This observation provides further validation for the ability of sedimentary I/TOC to record paleoredox and hence the potential for similar applications in more ancient sediments such as those deposited during OAE 2.

4.4. Oceanographic patterns of I/TOC during pre- and post-OAE 2 intervals

We report I/TOC and I_{org} data across OAE 2 deposits at six sites (Fig. 2). $\delta^{13}C$ and TOC data are plotted for each site (Fig. 6). Firstly, we discuss the spatial pattern of I/TOC during the background—that is, above and below the OAE 2 sediment. Subsequently, we discuss the temporal changes of I/TOC at individual sites. A summary of multiple redox proxies for each site can be found in Table 1.

I/TOC values for the pre- and post-OAE intervals display a wide range, from ~1 to >50 μmol/mol, effectively separating the study sites into two groups. Sites with background I/TOC

<5 μmol/mol appear to be located at low latitudes (Tarfaya, Furlo and Demerara Rise), with the exception of the Cape Verde Basin. Based on these contrasting I/TOC values, we suggest that bottom water was more oxic at the high-latitude sites and Cape Verde Basin, before and after the OAE, whereas most low-latitude sites had relatively oxygen-depleted bottom waters.

Two sites at higher latitudes (Kerguelen Plateau and South Ferriby) display background I/TOC of ~15–50 μmol/mol. Benthic foraminiferal assemblages at Kerguelen Plateau suggest that the bottom water might have been generally oxygenated with episodes of short-term dysoxic conditions (Coffin et al., 2000; Holbourn and Kuhnt, 2002). The independently suggested predominance of oxygenated conditions is in agreement with relatively high I/TOC values at this site. No proxy data are available in the literature directly addressing the bottom-water conditions at South Ferriby, although several studies imply a latitudinal increase of oxygenation on the seafloor from tropical sites to both North Atlantic and Northern Tethyan margins (Kuhnt and Wiedmann, 1995; Westermann et al., 2010; van Helmond et al., 2014; Westermann et al., 2014). The high I/TOC at South Ferriby (northernmost Atlantic site, in the European pelagic shelf sea) agrees with such a pattern. The background I/TOC at Cape Verde Basin is about 10–20 μmol/mol, lower than the range for Kerguelen Plateau and South Ferriby, indicating less oxic bottom waters before the OAE. Fe_{HR}/Fe_T values were steadily near 0.38 during that time (Westermann et al., 2014), representing a transitional state between the oxic and anoxic end-member sites, consistent with its intermediate I/TOC values among the six sites.

Elevated redox-sensitive trace-metal concentrations and repetitive deposition of laminated organic-rich sediments indicate suboxic to anoxic bottom water in the Tarfaya Basin (Kolonic et al., 2005), and the presence of isorenieratane and the high degree of pyritization in sediments indicate at least intermittent photic-zone euxinia at this site (Kolonic et al., 2005;

Poulton et al., 2015). Fe-speciation data also suggest bottom-water anoxia existed before OAE 2 at Tarfaya (Poulton et al., 2015), which agrees with the low I/TOC values determined in this study. In general, the low I/TOC background values at Tarfaya are consistent with the suggestions of less oxygenated bottom waters at this site before and after the event. Transient occurrences of relatively oxic bottom waters, suggested by much higher resolution studies (Kolonic et al., 2005; Kuhnt et al., 2005; Keller et al., 2008), are not captured in our low-resolution I/TOC record.

I/TOC values are relatively low in sediments deposited before, during and after OAE 2 at Demerara Rise and Furlo, consistent with anoxic conditions as suggested by trace metal data, $\delta^{15}N$, biomarkers and Fe-speciation results at these two sites (Owens et al., 2016 and 2017; Hetzel et al., 2009; Turgeon and Brumsack, 2006). The presence of the biomarkers isorenieratane and chlorobactane suggest photic-zone euxinia during OAE 2 at the relatively shallow Site 1260 on Demerara Rise, where lycopane to n-alkane ratios much higher than those in modern OMZs indicate prolonged anoxia in the bottom water throughout late Cenomanian to early Turonian (van Bentum et al., 2009). Similarly at Furlo, Fe speciation and Mo concentrations in black shales are consistent with intermittent local ferruginous conditions prior to the event and euxinic conditions during the OAE itself (Owens et al., 2016; Bunte, 2009; Westermann et al., 2014; Jenkyns et al., 2007).

4.5. Temporal changes in local I/TOC during OAE 2

OAE 2 sediments, as defined by the $\delta^{13}C$ excursion, show lower I/TOC at all study sites (Fig. 6), most likely indicating widespread increase in planktonic carbon flux and less oxygenated bottom-water conditions. The two high-latitude sites, Kerguelen and South Ferriby,

have minimum I/TOC values of ~10-25 μmol/mol during the OAE interval, which are significantly higher than the minimum I/TOC values at other sites (0–5 μmol/mol). Therefore, it seems likely that the relatively more oxygenated bottom waters found at higher latitudes persisted during the OAE itself.

The extent and timing of upper-ocean oxygenation changes indicated by I/Ca are commonly not synchronous when calibrated against the carbon-isotope curve that characterizes OAE 2 (Zhou et al., 2015). Compared to I/Ca records for near surface water conditions, I/TOC values for bottom water signals show slightly better covariance with the $\delta^{13}C$ profile through the OAE interval at almost all sites. It suggests that local bottom-water redox conditions were more synchronized to global organic-carbon burial. This result is unsurprising, because upper-ocean oxygenation (I/Ca) is heavily influenced by interactions with the atmosphere and ocean circulation, whereas bottom-water oxygenation during the OAE should reflect widespread organic-matter burial and oxygen consumption in the oceanic interior.

4.6. I/TOC *vs* modeled seafloor oxygen

The latitudinal oceanographic pattern of background I/TOC agrees with the bottom-water oxygenation simulated in Earth System Model cGENIE for the Late Cretaceous with a deeper Panama (Fig. 7)(Monteiro et al., 2012). The three sites with high I/TOC values (Kerguelen Plateau, South Ferriby, and Cape Verde Basin) were located in or near areas with modeled bottom-water oxygen higher than 100 μmol/l (pre-OAE), whereas the other three sites are in areas with modeled seafloor oxygen below 50 μmol/l. Most parts of the proto-North Atlantic were probably anoxic in the late Cretaceous, because the deep water in North Atlantic was likely

formed at relatively low latitudes during the Cretaceous Period, hence containing less oxygen (Monteiro et al., 2012).

In the model of Monteiro et al. (2012), the northeast corner of the proto-Atlantic had relatively oxic water extending from the surface ocean to ~0.5 km (Zhou et al., 2015), consistent with the highest I/TOC at South Ferriby (Fig. 7). Kerguelen Plateau was located at high southern latitudes, where less extreme temperatures could have favored higher levels of dissolved oxygen in seawater and possible formation of bottom water near this location. Nd-isotope results suggest deep-water formation in the Indian sector of the Southern Ocean at least from the late Albian to the late Cenomanian (Murphy and Thomas, 2012), which may have delivered O_2-rich deep water to Kerguelen, recorded as high I/TOC at this site.

The background I/TOC values (>10 μmol/mol) at Cape Verde are higher than expected, considering its low-latitude location. Interestingly, a modeled high O_2 anomaly on the seafloor appeared persistently at the equatorial Western African margin, even in reconstructions where high-latitude bottom waters became almost anoxic (Monteiro et al., 2012). Regardless of the relatively high background I/TOC, given low pre-OAE Fe_{HR}/Fe_T and Mo/TOC ratios (Westermann et al., 2014) and the proximity to the modeled bottom-water O_2 anomaly, the Cape Verde region was probably susceptible to the influence of anoxic bottom water, as suggested by rapidly declining I/TOC during the OAE that, in the mid-stage of the event, reached levels similar to those at Demerara Rise.

4.7. Seawater iodine inventory

The marine iodine inventory could have changed during the OAE 2 global organic-carbon burial event, since the main output of iodine from seawater is organic matter in marine

sediments (Muramatsu and Wedepohl, 1998). There is no consensus as to whether iodine would be drawn down as was the case with redox-sensitive trace metals (Algeo, 2004; Ma, et al., 2014; Owens et al., 2016) or whether it would be more efficiently remobilized and recycled like phosphate (Mort et al., 2007b), regardless of differences in remobilization mechanisms. The iodine budget has implications for the interpretation of the carbonate I/Ca record because I/Ca values are affected by the total iodine concentrations in seawater (IO_3^- + I^-). Organically bound iodine concentrations (I_{org}) may record, at least in part, the amount of buried iodine during OAE 2.

Average I_{org} values are highest at the Kerguelen and Cape Verde sites (Fig. 6). South Ferriby has relatively low I_{org} and low TOC, although it likely was well-oxygenated. These observations may indicate that the ideal sedimentary iodine sink in global ocean is relatively oxic and organic-rich settings, because strong iodine enrichments in surface sediments may require both high bottom water iodate concentrations and also abundant organic matters on seafloor as "substrate" to incorporate iodine. In this scenario, global marine iodine budget may be stabilized by the negative feedback between increasing organic matter production and decreasing oxic seafloor. I_{org} was elevated at Kerguelen and Cape Verde during the OAE, regardless of decreasing I/TOC, possibly due to stronger iodine enrichment driven by more abundant organic matter on the seafloor, overpowering the effect of deoxygenation (lower bottom water iodate level). I_{org} shows better correlation with TOC at Kerguelen and South Ferriby than at other sites during OAE 2, which may suggest that TOC becomes the main control for iodine enrichment when the bottom water is oxygenated (Fig. 8). At Furlo, Demerara Rise and Tarfaya, I_{org} values either remain at the same level as those of the pre-OAE interval or decrease during the OAE. Thus, regions with more reducing bottom waters (i.e. low iodate level) were not able to enhance

iodine burial given higher local fluxes of organic matter, further supporting the idea that both bottom water iodate and organic matters are requisites for an efficient sedimentary iodine sink. I_{org} and I/TOC are discussed separately as indicators for iodine inventory and oceanic oxygenation, respectively, but these parameters are likely influenced by both iodine budget and bottom water O_2, and even additional factors (e.g., sedimentation rates). Quantitative reconstructions teasing apart these intertwined changes during the OAE would require more future work.

5. Conclusions

I/TOC correlates with bottom-water oxygenation as an empirical relationship in the modern ocean, although the mechanism is not clearly understood. We developed a method to extract organic iodine from small volumes of sediments to explore the potential of I/TOC as a paleo-redox proxy. This proxy was first tested in Holocene Baltic sediments. The results indicate that I/TOC is sensitive to hypoxic-anoxic conditions, potentially as a useful addition to existing well-established metal proxies for anoxic-euxinic conditions. I/TOC data from six sites across the Cenomanian–Turonian OAE 2 showed relatively more oxic conditions at high-latitude sites, consistent with other redox indicators and model simulations. Bottom waters became more reducing during OAE 2 at all sites, as illustrated by lower I/TOC values. Compared to upper-ocean oxygenation indicated by carbonate I/Ca, temporal changes in bottom-water conditions were relatively synchronous with global organic-carbon burial and oxygen utilization in the ocean interior during OAE 2. Total organically bound iodine content (I_{org}) did not show consistent changes through the OAE 2 interval at different sites, therefore no firm conclusions as to the possible extent of global iodine burial can be drawn from the available data. Relatively

484 organic-rich sediments deposited under oxygenated bottom-water conditions may be an
485 important sink for seawater iodine on global scale.
486
487 **Acknowledgements**
488 XZ, WL and ZL are supported by NSF EAR 1349252. DH and TWL acknowledge support from
489 the Geobiology and Low-temperature Geochemistry (GG) Program of NSF. DH would like to
490 acknowledge a Schlanger Ocean Drilling Fellowship.
491
492
493 **References**
494 Adams, D.D., Hurtgen, M.T., and Sageman, B.B., 2010, Volcanic triggering of a biogeochemical
495 cascade during Oceanic Anoxic Event 2: Nature Geoscience, v. 3, no. 3, p. 201–204, doi:
496 Doi 10.1038/Ngeo743.
497 Algeo, T.J., 2004, Can marine anoxic events draw down the trace element inventory of seawater?
498 Geology, v. 32, no. 12, p. 1057–1060, doi: 10.1130/G20896.1.
499 Algeo, T.J., and Lyons, T.W., 2006, Mo-total organic carbon covariation in modern anoxic
500 marine environments: Implications for analysis of paleoredox and paleohydrographic
501 conditions: Paleoceanography, v. 21, no. 1, doi: 10.1029/2004PA001112.
502 Algeo, T.J., and Tribovillard, N., 2009, Environmental analysis of paleoceanographic systems
503 based on molybdenum-uranium covariation: Chemical Geology, v. 268, no. 3-4, p. 211–225,
504 doi: 10.1016/j.chemgeo.2009.09.001.
505 Andrén, T., Jørgensen, B.B., Cotterill, C., Green, S., Andrén, E., Ash, J., Bauersachs, T., Cragg,
506 B., Fanget, A.-S., Fehr, A., Granoszewski, W., Groeneveld, J., Hardisty, D., Herrero-

507 Bervera, E., Hyttinen, O., Jensen, J.B., Johnson, S., Kenzler, M., Kotilainen, A., Kotthoff,
508 U., Marshall, I.P.G., Martin, E., Obrochta, S., Passchier, S., Quintana Krupinski, N.,
509 Riedinger, N., Slomp, C., Snowball, I., Stepanova, A., Strano, S., Torti, A., Warnock, J.,
510 Xiao, N., and Zhang, R., 2015. Site M0063. In Andrén, T., Jørgensen, B.B., Cotterill, C.,
511 Green, S., and the Expedition 347 Scientists, Proc. IODP, 347: College Station, TX
512 (Integrated Ocean Drilling Program). doi:10.2204/iodp.proc.347.107.2015
513 Arthur, M.A., Dean, W.E., and Pratt, L.M., 1988, Geochemical and climatic effects of increased
514 marine organic carbon burial at the Cenomanian/Turonian boundary: Nature, v. 335, p.
515 714–717.
516 Arthur, M.A., Jenkyns, H.C., Brumsack, H.J., and Schlanger, S.O., 1990, Stratigraphy,
517 geochemistry, and paleoceanography of organic carbon-rich Cretaceous sequences, *in*
518 Ginsburg, R.N. and Beaudoin, B. eds., Cretaceous Resources, Events and Rhythms, Kluwer
519 Academic Publishers, p. 75–119.
520 Barclay, R.S., McElwain, J.C., and Sageman, B.B., 2010, Carbon sequestration activated by a
521 volcanic CO_2 pulse during Ocean Anoxic Event 2: Nature Geoscience, v. 3, p. 205-208,
522 doi:10.1038/ngeo757.
523 van Bentum, E.C., Hetzel, A., Brumsack, H.J., Forster, A., Reichart, G.J., and Damste, J.S.S.,
524 2009, Reconstruction of water column anoxia in the equatorial Atlantic during the
525 Cenomanian-Turonian oceanic anoxic event using biomarker and trace metal proxies:
526 Palaeogeography Palaeoclimatology Palaeoecology, v. 280, no. 3-4, p. 489–498, doi: DOI
527 10.1016/j.palaeo.2009.07.003.
528 Blattler, C.L., Jenkyns, H.C., Reynard, L.M., and Henderson, G.M., 2011, Significant increases
529 in global weathering during Oceanic Anoxic Events 1a and 2 indicated by calcium isotopes:

Earth and Planetary Science Letters, v. 309, no. 1-2, p. 77–88, doi: 10.1016/j.epsl.2011.06.029.

Bluhm, K., Croot, P.L., Huhn, O., Rohardt, G., and Lochte, K., 2011, Distribution of iodide and iodate in the Atlantic sector of the southern ocean during austral summer: Deep-Sea Research Part Ii-Topical Studies in Oceanography, v. 58, no. 25-26, p. 2733–2748, doi: 10.1016/j.dsr2.2011.02.002.

Bomou, B., Adatte, T., Tantawy, A.A., Mort, H., Fleitmann, D., Huang, Y., and Föllmi, K.B., 2013, The expression of the Cenomanian-Turonian oceanic anoxic event in Tibet: Palaeogeography, Palaeoclimatology, Palaeoecology, v. 369, p. 466–481, doi: 10.1016/j.palaeo.2012.11.011.

Brewer, P.G., Nozaki, Y., Spencer, D.W., and Fleer, A.P., 1980, SEDIMENT TRAP EXPERIMENTS IN THE DEEP NORTH-ATLANTIC - ISOTOPIC AND ELEMENTAL FLUXES: Journal of Marine Research, v. 38, no. 4, p. 703–728.

Brown, C.F., Geiszler, K.N., and Vickerman, T.S., 2005, Extraction and quantitative analysis of iodine in solid and solution matrixes.: Analytical chemistry, v. 77, no. 21, p. 7062–6, doi: 10.1021/ac050972v.

Bunte, von F.A., 2009, Geochemical signatures of black shales deposited during Oceanic Anoxic Event 2 (Cenomanian/Turonian) in the tropical Atlantic (Demerara Rise, ODP Leg 207) and in northern Germany (Wunstorf): Carl von Ossietzky Universität Oldenburg.

Chenet, P.Y., and Francheteau, J., 1979, Bathymetric reconstruction method: application to the Central Atlantic Basin between 10◦N and 40◦N: Initial Reports of the Deep Sea Drilling Project, v. 51-53, p. 1501–1514.

Coffin, M.F., Frey, F.A., and Wallace, P.J., 2000, 6. Site 1138: Proceedings of the Ocean

553 Drilling Program, Initial Reports, v. 183.
554 Dashtgard, S.E., MacEachern, J.A., 2016. Unburrowed mudstones may record only slightly
555 lowered oxygen conditions in warm, shallow basins. Geology 44, G37648.1.
556 doi:10.1130/G37648.1
557 Demaison, G.J., Moore, G.T., 1980. Anoxic environments and oil source bed genesis. Organic
558 Geochemistry, v. 2, pp.9–31.
559 Elderfield, H., and Truesdale, V.W., 1980, On the Biophilic Nature of Iodine in Seawater: Earth
560 and Planetary Science Letters, v. 50, no. 1, p. 105–114.
561 El-Sabbagh, A., Tantawy, A.A., Keller, G., Khozyem, H., Spangenberg, J., Adatte, T., and
562 Gertsch, B., 2011, Stratigraphy of the Cenomanian–Turonian Oceanic Anoxic Event OAE 2
563 in shallow shelf sequences of NE Egypt: Cretaceous Research, v. 32, no. 6, p. 705–722, doi:
564 10.1016/j.cretres.2011.04.006.
565 Erbacher, J., Friedrich, O., Wilson, P.A., Birch, H., and Mutterlose, J., 2005, Stable organic
566 carbon isotope stratigraphy across Oceanic Anoxic Event 2 of Demerara Rise, western
567 tropical Atlantic: Geochemistry Geophysics Geosystems, v. 6, doi: 10.1029/2004gc000850.
568 Erbacher, J., Mosher, D.C., and Malone, M.J., 2004, 5. Site 1258: Proceedings of the Ocean
569 Drilling Program Initial Reports, v. 207.
570 Farrenkopf, A.M., Luther, G.W., 2002. Iodine chemistry reflects productivity and denitrification
571 in the Arabian Sea: evidence for flux of dissolved species from sediments of western India
572 into the OMZ. Deep. Res. Part Ii-Topical Stud. Oceanogr. 49, 2303–2318.
573 Francois, R., 1987. The influence of humic substances on the geochemistry of iodine in
574 nearshore and hemipelagic marine-sediments. Geochim. Cosmochim. Acta 51, 2417–2427.
575 Friedrich, O., Erbacher, J., and Mutterlose, J., 2006, Paleoenvironmental changes across

576 the Cenomanian/Turonian Boundary Event (Oceanic Anoxic Event 2) as indicated
577 by benthic foraminifera from the Demerara Rise (ODP Leg 207): Revue de
578 Micropaléontologie, v. 49, no. 3, p. 121–139, doi: 10.1016/j.revmic.2006.04.003.
579 Gambacorta, G., Jenkyns, H.C., Russo, F., Tsikos, H., Wilson, P.A., Faucher, G. and Erba, E.,
580 2015, Carbon- and oxygen-isotope records of mid-Cretaceous Tethyan pelagic sequences
581 from the Umbria–Marche and Belluno Basins (Italy). Newsletters Stratigr., 48, 299–323.
582 Gertsch, B., Keller, G., Adatte, T., Berner, Z., Kassab, A., Tantawy, A., El-Sabbagh, A., and
583 Stueben, D., 2010, Cenomanian–Turonian transition in a shallow water sequence of the
584 Sinai, Egypt: International Journal of Earth Sciences, v. 99, no. 1, p. 165–182, doi:
585 10.1007/s00531-008-0374-4.
586 Grimm, M.R., 1952, Iodine Content of Some Marine Algae: Cornell University, 318–323 p.
587 van Helmond, N.A.G.M., Ruvalcaba Baroni, I., Sluijs, A., Sinninghe Damsté, J.S., and Slomp,
588 C.P., 2014, Spatial extent and degree of oxygen depletion in the deep proto-North Atlantic
589 basin during Oceanic Anoxic Event 2: Geochemistry, Geophysics, Geosystems, v. 15, p.
590 4254–4266, doi: 10.1002/2014GC005528.
591 Hasegawa, T., 1997, Cenomanian-Turonian carbon isotope events recorded in terrestrial organic
592 matter from northern Japan. Palaeogeography, Palaeoclimatology, Palaeoecology, v. 130, p.
593 251–273.
594 Hardisty, D.S., Riedinger, N., Planavsky, N.J., Asael, D., Andrén, T., Jørgensen, B.B., and Lyons,
595 T.W., 2016, A Holocene history of dynamic water column redox conditions in the Landsort
596 Deep, Baltic Sea (IODP Expedition 347). American Journal of Science 216, 713–745.
597 Hetzel, A., Bottcher, M.E., Wortmann, U.G., and Brumsack, H.J., 2009, Paleo-redox conditions
598 during OAE 2 reflected in Demerara Rise sediment geochemistry (ODP Leg 207):

599 Palaeogeography Palaeoclimatology Palaeoecology, v. 273, p. 302–328, doi: DOI
600 10.1016/j.palaeo.2008.11.005.
601 Hetzel, A., März, C., Vogt, C., and Brumsack, H.J., 2011, Geochemical environment of
602 Cenomanian - Turonian black shale deposition at Wunstorf (northern Germany): Cretaceous
603 Research, v. 32, no. 4, p. 480–494, doi: 10.1016/j.cretres.2011.03.004.
604 Holbourn, A., and Kuhnt, W., 2002, Cenomanian–Turonian palaeoceanographic change on the
605 Kerguelen Plateau: a comparison with Northern Hemisphere records: Cretaceous Research,
606 v. 23, no. 3, p. 333–349, doi: 10.1006/cres.2002.1008.
607 Jarvis, I., Lignum, J.S., Gröcke, D.R., Jenkyns, H.C., and Pearce, M.A., 2011, Black shale
608 deposition, atmospheric CO_2 drawdown and cooling during the Cenomanian-Turonian
609 Oceanic Anoxic Event (OAE 2): Paleoceanography, v. 26, no. 3, p. PA3201, doi:
610 10.1029/2010PA002081.
611 Jenkyns, H.C., 1980. Cretaceous anoxic events: from continents to oceans. Journal of the
612 Geological Society, v. 137, p. 171–188.
613 Jenkyns, H.C., 2003, Evidence for rapid climate change in the Mesozoic-Palaeogene greenhouse
614 world: Philosophical Transactions of the Royal Society a-Mathematical Physical and
615 Engineering Sciences, v. 361, no. 1810, p. 1885–1916, doi: 10.1098/rsta.2003.1240.
616 Jenkyns, H.C., 2010, Geochemistry of oceanic anoxic events: Geochemistry Geophysics
617 Geosystems, v. 11, doi: 10.1029/2009gc002788.
618 Jenkyns, H.C., Matthews, A., Tsikos, H., and Erel, Y., 2007, Nitrate reduction, sulfate reduction,
619 and sedimentary iron isotope evolution during the Cenomanian-Turonian oceanic anoxic
620 event: Paleoceanography, v. 22, no. 3, doi: 10.1029/2006pa001355.
621 Jenkyns, H.C., Dickson, A.J., Ruhl, M. & van den Boorn, S.H.J.M., (2017). Basalt–seawater

622 interaction, the Plenus Cold Event, enhanced weathering and geochemical change:
623 deconstructing Oceanic Anoxic Event 2 (Cenomanian–Turonian, Late Cretaceous).
624 Sedimentology, 64, doi: 10.1111/sed.12305, in press.
625 Jones, E.J.W., Bigg, G.R., Handoh, I.C., and Spathopoulos, F., 2007, Distribution of deep-sea
626 black shales of Cretaceous age in the eastern Equatorial Atlantic from seismic profiling:
627 Palaeogeography, Palaeoclimatology, Palaeoecology, v. 248, no. 1-2, p. 233–246, doi:
628 10.1016/j.palaeo.2006.12.006.
629 Jones, C.E., and Jenkyns, H.C., 2001, Seawater strontium isotopes, oceanic anoxic events, and
630 seafloor hydrothermal activity in the Jurassic and Cretaceous: American Journal of Science,
631 v. 301, no. 2, p. 112–149.
632 Junium, C.K., Freeman, K.H., and Arthur, M.A., 2015, Controls on the stratigraphic distribution
633 and nitrogen isotopic composition of zinc, vanadyl and free base porphyrins through
634 Oceanic Anoxic Event 2 at Demerara Rise: Organic Geochemistry, v. 80, p. 60-71,
635 doi:10.1016/j.orggeochem.2014.10.009.
636 Keller, G., Adatte, T., Berner, Z., Chellai, E.H. and Stueben, D., 2008. Oceanic events and biotic
637 effects of the Cenomanian-Turonian anoxic event, Tarfaya Basin, Morocco. *Cretaceous*
638 *Research*, *29*(5), pp.976-994.
639 Kennedy, H.A., and Elderfield, H., 1987a, Iodine Diagenesis in Non-Pelagic Deep-Sea
640 Sediments: Geochimica et Cosmochimica Acta, v. 51, no. 9, p. 2505–2514.
641 Kennedy, H.A., and Elderfield, H., 1987b, Iodine Diagenesis in Pelagic Deep-Sea Sediments:
642 Geochimica et Cosmochimica Acta, v. 51, no. 9, p. 2489–2504.
643 Kerr, A.C., 1998, Oceanic plateau formation: a cause of mass extinction and black shale
644 deposition around the Cenomanian-Turonian boundary? Journal of the Geological Society,

v. 155, p. 619–626, doi: 10.1144/gsjgs.155.4.0619.

Knapp, G., Maichin, B., Fecher, P., Hasse, S., and Schramel, P., 1998, Iodine determination in biological materials: Options for sample preparation and final determination: Journal of Analytical Chemistry, v. 362, no. 6, p. 508–513.

Kolonic, S., Wagner, T., Forster, A., Sinninghe Damsté, J.S., Walsworth-Bell, B., Erba, E., Turgeon, S., Brumsack, H.-J., Chellai, E.H., Tsikos, H., Kuhnt, W., and Kuypers, M.M.M., 2005, Black shale deposition on the northwest African Shelf during the Cenomanian/Turonian oceanic anoxic event: Climate coupling and global organic carbon burial: Paleoceanography, v. 20, no. 1, p. PA1006, doi: 10.1029/2003PA000950.

Kuhnt, W., Luderer, F., Nederbragt, S., Thurow, J., and Wagner, T., 2005, Orbital-scale record of the late Cenomanian-Turonian oceanic anoxic event (OAE-2) in the Tarfaya Basin (Morocco): International Journal of Earth Sciences, v. 94, p. 147–159, doi: 10.1007/s00531-004-0440-5.

Kuhnt, W., and Wiedmann, J., 1995, Cenomanian-Turonian source rocks: paleobiogeographic and paleoenvironmental aspects: AAPG, Studies in Geology, v. 40, p. 213–231.

Kuroda, J., Ogawa, N.O., Tanimizu, M., Coffin, M.F., Tokuyama, H., Kitazato, H., and Ohkouchi, N., 2007, Contemporaneous massive subaerial volcanism and late cretaceous Oceanic Anoxic Event 2: Earth and Planetary Science Letters, v. 256, no. 1-2, p. 211–223, doi: 10.1016/j.epsl.2007.01.027.

Kuypers, M.M.M., Pancost, R.D., Nijenhuis, I.A., and Damste, J.S.S., 2002, Enhanced productivity led to increased organic carbon burial in the euxinic North Atlantic basin during the late Cenomanian oceanic anoxic event: Paleoceanography, v. 17, no. 4, doi: 10.1029/2000pa000569.

668 Lancelot, Y., Seibold, E., Cepek, P., Dean, W.E., Eremeev, V., Gardner, J., Jansa, L.F., Johnson,
669 D., Krasheninnikov, V., Pflaumann, U., Rankin, J.G., Trabant, P., and Bukry, D., 1977, Site
670 367: Cape Verde Basin: Deep Sea Drilling Project Initial Reports, v. 41, no. March, p. 163–
671 232.
672 Lanci, L., Muttoni, G., and Erba, E., 2010, Astronomical tuning of the Cenomanian Scaglia
673 Bianca Formation at Furlo, Italy: Earth and Planetary Science Letters, v. 292, no. 1-2, p.
674 231–237, doi: 10.1016/j.epsl.2010.01.041.
675 Leine , L., 1986, Geology of the Tarfaya oil shale deposit, Morocco: Geologie en Mijnbouw, v.
676 65, p. 57–74.
677 Lu, Z., Hensen, C., Fehn, U., and Wallmann, K., 2008, Halogen and 129I systematics in gas
678 hydrate fields at the northern Cascadia margin (IODP Expedition 311): Insights from
679 numerical modeling: Geochemistry, Geophysics, Geosystems, v. 9, doi:
680 10.1029/2008GC002156.
681 Lu, Z., Jenkyns, H.C., Rickaby, R.E.M., 2010. Iodine to calcium ratios in marine carbonate as a
682 paleo-redox proxy during oceanic anoxic events. Geology 38, 1107–1110.
683 doi:10.1130/G31145.1
684 Ma, C., Meyers, S. R., Sageman, B. B., Singer, B. S., and Jicha, B. R., 2014, Testing the
685 astronomical time scale for oceanic anoxic event 2, and its extension into Cenomanian strata
686 of the Western Interior Basin (USA): GSA Bulletin; v. 126, no. 7-8, p. 974–989, doi:
687 10.1130/B30922.1.
688 Mitchell, R.N., Bice, D.M., Montanari, A., Cleaveland, L.C., Christianson, K.T., Coccioni, R.,
689 and Hinnov, L.A., 2008, Oceanic anoxic cycles? Orbital prelude to the Bonarelli Level
690 (OAE 2): Earth and Planetary Science Letters, v. 267, no. 1-2, p. 1–16, doi:

691 10.1016/j.epsl.2007.11.026.
692 Monteiro, F.M., Pancost, R.D., Ridgwell, A., and Donnadieu, Y., 2012, Nutrients as the
693 dominant control on the spread of anoxia and euxinia across the Cenomanian-Turonian
694 oceanic anoxic event (OAE 2): Model-data comparison: Paleoceanography, v. 27, doi:
695 10.1029/2012pa002351.
696 Mort, H., Jacquat, O., Adatte, T., Steinmann, P., Föllmi, K., Matera, V., Berner, Z., and Stüben,
697 D., 2007a, The Cenomanian/Turonian anoxic event at the Bonarelli Level in Italy and Spain:
698 enhanced productivity and/or better preservation? Cretaceous Research, v. 28, no. 4, p. 597–
699 612, doi: 10.1016/j.cretres.2006.09.003.
700 Mort, H.P., Adatte, T., Follmi, K.B., Keller, G., Steinmann, P., Matera, V., Berner, Z., and
701 Stuben, D., 2007b, Phosphorus and the roles of productivity and nutrient recycling during
702 oceanic anoxic event 2: Geology, v. 35, no. 6, p. 483–486, doi: Doi 10.1130/G23475a.1.
703 Muramatsu, Y., and Wedepohl, K.H., 1998, The distribution of iodine in the earth's crust:
704 Chemical Geology, v. 147, no. 3-4, p. 201–216.
705 Murphy, D.P., and Thomas, D.J., 2012, Cretaceous deep-water formation in the Indian sector of
706 the Southern Ocean: Paleoceanography, v. 27, no. 1, p. PA1211, doi:
707 10.1029/2011PA002198.
708 Nederbragt, A.J., Thurow, J., and Pearce, R., 2007, Sediment composition and cyclicity in the
709 Mid-Cretaceous at Demerara Rise, ODP Leg 207: Proc. ODP Sci. Results, v. 207, p. 1–31,
710 doi: 10.2973/odp.proc.sr.207.103.2007.
711 Owens, J.D., Lyons, T.W., Li, X., MacLeod, K.G., Gordon, G., Kuypers, M.M.M., Anbar, A.,
712 Kuhnt, W., and Severmann, S., 2012, Iron isotope and trace metal records of iron cycling in
713 the proto-North Atlantic during the Cenomanian-Turonian oceanic anoxic event (OAE-2):

714 Paleoceanography, v. 27, no. 3, p. 1–13, doi: 10.1029/2012PA002328.
715 Owens, J.D., Christopher T. Reinhard, Megan Rohrssen, Gordon D. Love, Timothy W. Lyons,
716 2016, Empirical links between trace metal cycling and marine microbial ecology during a
717 large perturbation to Earth's carbon cycle: Earth and Planetary Science Letters, v. 449, p.
718 407-417.
719 Owens, J.D., Lyons, T.W., Hardisty, D.S., Lowery, C., Lu, Z., Lee, B., and Jenkyns H.C., 2017,
720 Patterns of local and global redox variability during the Cenomanian–Turonian Boundary
721 Event (OAE 2) recorded in carbonates and shales from central Italy: Sedimentology.
722 Pancost, R.D., Crawford, N., Magness, S., Turner, A., Jenkyns, H.C., and Maxwell, J.R., 2004,
723 Further evidence for the development of photic-zone euxinic conditions during Mesozoic
724 oceanic anoxic events: Journal of the Geological Society, v. 161, p. 353–364.
725 Pogge von Strandmann, P.A.E., Jenkyns, H.C., and Woodfine, R.G., 2013, Lithium isotope
726 evidence for enhanced weathering during Oceanic Anoxic Event 2: Nature Geoscience, v. 6,
727 no. 8, p. 668–672, doi: 10.1038/ngeo1875.
728 Poulton, S.W., and Canfeld, D.E., 2011, Ferruginous conditions: A dominant feature of the ocean
729 through Earth's history: Elements, v. 7, no. 2, p. 107–112, doi: 10.2113/gselements.7.2.107.
730 Poulton, S.W., and Canfield, D.E., 2005, Development of a sequential extraction procedure for
731 iron: Implications for iron partitioning in continentally derived particulates: Chemical
732 Geology, v. 214, no. 3-4, p. 209–221, doi: 10.1016/j.chemgeo.2004.09.003.
733 Poulton, S.W., Henkel, S., März, C., Urquhart, H., Flögel, S., Kasten, S., Sinninghe Damsté, J.S.,
734 and Wagner, T., 2015, A continental-weathering control on orbitally driven redox-nutrient
735 cycling during Cretaceous Oceanic Anoxic Event 2: Geology, v. 43, no. 11, p. 963–966, doi:
736 10.1130/G36837.1.

737 Price, N.B., and Calvert, S.E., 1973, Geochemistry of iodine in oxidized and reduced recent
738 marine sediments: Geochimica et Cosmochimica Acta, v. 37, no. 9, p. 2149–2158, doi:
739 10.1016/0016-7037(73)90013-6.
740 Price, N.B., and Calvert, S.E., 1977, The contrasting geochemical behaviours of iodine and
741 bromine in recent sediments from the Namibian shelf: Geochimica et Cosmochimica Acta,
742 v. 41, no. 12, p. 1769–1775, doi: 10.1016/0016-7037(77)90209-5.
743 Price, N.B., Calvert, S. E., and Jones, P.G.W., 1970, The distribution of iodine and bromine in
744 the sediments of the Southwestern Barents Sea: Journal of Marine Research, v. 28, no. 1, p.
745 22–34.
746 Reolid, M., Sánchez-Quiñónez, C. a., Alegret, L., and Molina, E., 2015, Palaeoenvironmental
747 turnover across the Cenomanian-Turonian transition in Oued Bahloul, Tunisia: foraminifera
748 and geochemical proxies: Palaeogeography, Palaeoclimatology, Palaeoecology, v. 417, p.
749 491–510, doi: 10.1016/j.palaeo.2014.10.011.
750 Romarís-Hortas, V., Moreda-Piñeiro, A., and Bermejo-Barrera, P., 2009, Microwave assisted
751 extraction of iodine and bromine from edible seaweed for inductively coupled plasma-mass
752 spectrometry determination: Talanta, v. 79, no. 3, p. 947–952, doi:
753 10.1016/j.talanta.2009.05.036.
754 Rue, E.L., Smith, G.J., Cutter, G.A., Bruland, K.W., 1997. The response of trace element redox
755 couples to suboxic conditions in the water column. Deep. Res. Part I-Oceanographic Res.
756 Pap. 44, 113–134.
757 Schlanger, S.O., Arthur, M.A., Jenkyns, H.C., and Scholle, P.A., 1987, The Cenomanian–
758 Turonian oceanic anoxic event, I. Stratigraphy and distribution of organic carbo-rich beds
759 and the marine d13C excursion, *in* Brooks, J. and Fleet, A.J. eds., Marine Petroleum Source

760 Rocks, p. 371–399.
761 Schlanger, S.O., and Jenkyns, H.C., 1976, Cretaceous oceanic anoxic events: causes and
762 consequences: Geol. Mijnb, v. 55, p. 179–194.
763 Scott, C., Lyons, T.W., 2012. Contrasting molybdenum cycling and isotopic properties in euxinic
764 versus non-euxinic sediments and sedimentary rocks: Refining the paleoproxies. Chem.
765 Geol. 324, 19–27. doi:10.1016/j.chemgeo.2012.05.012
766 Sinninghe Damste, J.S., and Koster, J., 1998, A euxinic southern North Atlantic Ocean during
767 the Cenomanian/Turonian oceanic anoxic event: Earth and Planetary Science Letters, v. 158,
768 no. 3-4, p. 165–173.
769 Takashima, R., Nishi, H., Hayashi, K., Okada, H., Kawahata, H., Yamanaka, T., Fernando, A.G.,
770 and Mampuku, M., 2009, Litho-, bio- and chemostratigraphy across the
771 Cenomanian/Turonian boundary (OAE 2) in the Vocontian Basin of southeastern France:
772 Palaeogeography, Palaeoclimatology, Palaeoecology, v. 273, no. 1-2, p. 61–74, doi:
773 10.1016/j.palaeo.2008.12.001.
774 Tinggi, U., Schoendorfer, N., Davies, P.S.W., Scheelings, P., and Olszowy, H., 2011,
775 Determination of iodine in selected foods and diets by inductively coupled plasma-mass
776 spectrometry: Pure and Applied Chemistry, v. 84, no. 2, p. 291–299, doi: 10.1351/PAC-
777 CON-11-08-03.
778 Topper, R.P.M., Alexandre, J.T., Tuenter, E., and Meijer, P.T., 2011, A regional ocean
779 circulation model for the mid-Cretaceous North Atlantic Basin: implications for black shale
780 formation: Climate of the Past, v. 7, no. 1, p. 277–297, doi: 10.5194/cp-7-277-2011.
781 Tsikos, H., Jenkyns, H.C., Walsworth-Bell, B., Petrizzo, M.R., Forster, A., Kolonic, S., Erba, E.,
782 Silva, I.P., Baas, M., Wagner, T., and Damste, J.S.S., 2004, Carbon-isotope stratigraphy

783 recorded by the Cenomanian-Turonian Oceanic Anoxic Event: correlation and implications
784 based on three key localities: Journal of the Geological Society, v. 161, p. 711–719.
785 Tsunogai, S., 1971, Iodine in the deep water of the ocean: Deep Sea Research and
786 Oceanographic Abstracts, v. 18, no. 9, p. 913–919, doi: 10.1016/0011-7471(71)90065-9.
787 Tsunogai, S., and Sase, T., 1969, Formation of Iodide-Iodine in Ocean: Deep-Sea Research, v.
788 16, no. 5, p. 489.
789 Tullai, S., Tubbs, L.E., and Fehn, U., 1987, Iodine Extraction from Petroleum for Analysis of I-
790 129/I-127 Ratios by Ams: Nuclear Instruments & Methods in Physics Research Section B-
791 Beam Interactions with Materials and Atoms, v. 29, no. 1-2, p. 383–386.
792 Turgeon, S.C., and Creaser, R.A., 2008, Cretaceous oceanic anoxic event 2 triggered by a
793 massive magmatic episode: Nature, v. 454, p. 323–329, doi: 10.1038/Nature07076.
794 Turgeon, S. and Brumsack, H.-J., 2006, Anoxic vs dysoxic events reflected in sediment
795 geochemistry during the Cenomanian–Turonian Boundary Event (Cretaceous) in the
796 Umbria–Marche Basin of central Italy. Chemical Geology, v. 234, p.321–339.
797 Ullman, W.J., and Aller, R.C., 1985, The Geochemistry of Iodine in near-Shore Carbonate
798 Sediments: Geochimica et Cosmochimica Acta, v. 49, no. 4, p. 967–978.
799 Waite, T.J., and Truesdale, V.W., 2003, Iodate reduction by Isochrysis galbana is relatively
800 insensitive to de-activation of nitrate reductase activity - are phytoplankton really
801 responsible for iodate reduction in seawater? Marine Chemistry, v. 81, no. 3-4, p. 137–148,
802 doi: 10.1016/s0304-4203(03)00013-6.
803 Westermann, S., Caron, M., Fiet, N., Fleitmann, D., Matera, V., Adatte, T., and Föllmi, K.B.,
804 2010, Evidence for oxic conditions during oceanic anoxic event 2 in the northern Tethyan
805 pelagic realm: Cretaceous Research, v. 31, no. 5, p. 500–514, doi:

10.1016/j.cretres.2010.07.001.

Westermann, S., Vance, D., Cameron, V., Archer, C., and Robinson, S.A., 2014, Heterogeneous oxygenation states in the Atlantic and Tethys oceans during Oceanic Anoxic Event 2: Earth and Planetary Science Letters, v. 404, p. 178–189, doi: 10.1016/j.epsl.2014.07.018.

Wong, G.T.F., 1980, The stability of dissolved inorganic species of iodine in seawater: Marine Chemistry, v. 9, no. 1, p. 13–24, doi: 10.1016/0304-4203(80)90003-1.

Zhou, X., Jenkyns, H.C., Owens, J.D., Junium, C.K., Zheng, X., Sageman, B.B., Hardisty, D.S., Lyons, T.W., Ridgwell, A., and Lu, Z., 2015, Upper ocean oxygenation dynamics from I/Ca ratios during the Cenomanian-Turonian OAE 2: Paleoceanography, v. 30, p. 510–526. doi:10.1002/2014PA002741.

Zillén, L., Conley, D.J., Andrén, T., Andrén, E., Björck, S., 2008. Past occurrences of hypoxia in the Baltic Sea and the role of climate variability, environmental change and human impact. Earth-Science Rev. 91, 77–92. doi:10.1016/j.earscirev.2008.10.001

821 **Tables**

822 Table 1. Summary of redox proxy observations for OAE 2 at study sites.

Site	Proxies	Pre-CIE	CIE	Post-CIE	References
Demerara Rise	I/Ca	Low I/Ca values			Zhou et al., 2015
	Trace metals	Low Mn content	Enrichment of Fe and Co, low Mn content	Low Mn content	Hetzel et al., 2009
	Biomarkers	Presence of lycopane	Presence of Isorenieratane, chlorobactane and lycopane	Presence of lycopane	van Bentum, 2009
	Foraminifera		Low abundance in benthic foraminifera		Friedrich et al., 2006
Tarfaya	I/Ca	Low I/Ca values	Low I/Ca values	Low I/Ca values	Zhou et al., 2015
	Iron speciation		Fe_{HR}/Fe_T higher than 0.38, Fe_{Py}/Fe_{HR} fluctuating around 0.7 (0.4-0.9)		Poulton et al., 2015
	Biomarkers		Presence of Isorenieratane and chlorobactane	Presence of Isorenieratane and chlorobactane	Kolonic et al., 2005; Poulton et al., 2015
	Foraminifera	Low abundance of benthic foraminifera			
Furlo	I/Ca	Low I/Ca values		Low I/Ca values	
	Iron speciation	Fe_{HR}/Fe_T higher than 0.38, Fe_{Py}/Fe_{HR} lower than 0.8	Fe_{HR}/Fe_T higher than 0.38, Fe_{Py}/Fe_{HR} lower than 0.8		Westermann et al., 2014
	Trace metals		High U, V, Mo contents, low Mn content		Turgeon and Brumsack, 2006
Cape Verde Basin	Iron speciation		Fe_{HR}/Fe_T higher than 0.38, Fe_{Py}/Fe_{HR} between 0.1 and 0.7		Westermann et al., 2014
	Trace metals	High V contents	High U, V, Mo contents		Westermann et al., 2014
Kerguelen Plateau	Foraminifera		Barren foraminifera		Holbourn and Kuhnt, 2002
South Ferriby	I/Ca	High I/Ca suggest relatively oxygenated upper ocean	I/Ca peaks may suggest local water oxygenation or invasion of iodate-rich waters	High I/Ca suggest relatively oxygenated upper ocean	Zhou et al., 2015
	Trace metals	High Mn content	Low Mn content suggest dysoxic bottom water	High Mn content	Turgeon and Brumsack, 2006

823

Figures

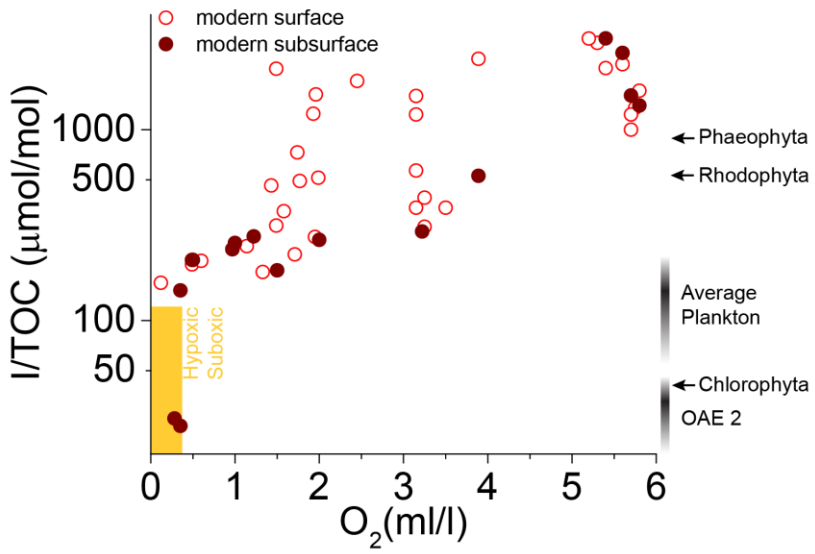

Figure 1. I/TOC of modern marine sediments plotted with bottom-water oxygen concentration immediately overlying the sea floor. The open circles are surface sediments of the southwest African continental shelf (Price and Calvert, 1973), tropical eastern Pacific and coastal areas of North Atlantic (Kennedy and Elderfield, 1987a). Closed circles are subsurface sediments from the Namibian shelf (Price and Calvert, 1977), Cascadia margin (Lu et al., 2008), and coastal areas of the tropical North Atlantic (Kennedy and Elderfield, 1987a). The highest I/TOC values in different groups of algae, average I/TOC values in plankton, and the range of OAE 2 I/TOC values are indicated as short arrows and a grey shading, respectively (Grimm, 1952).

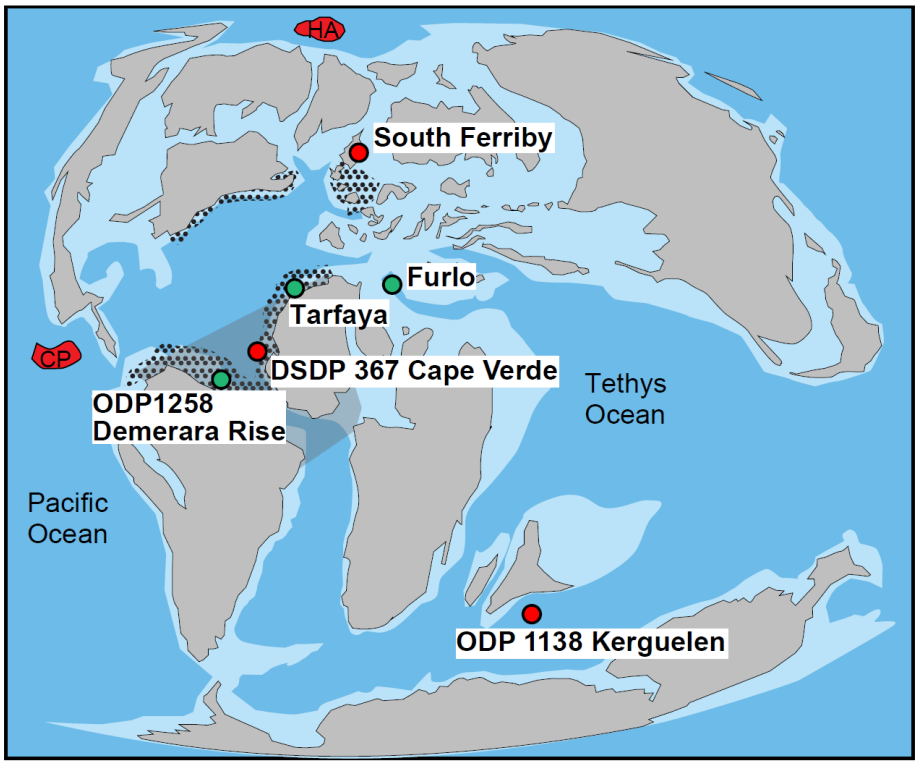

835

836 Figure 2. Paleogeographic map for the Late Cretaceous. The beige shading represents continents,
837 light blue neritic (shelf) seas, and dark blue deep sea. The six OAE 2 sections are divided into
838 two groups; the green circles represent relatively reducing locations, and the red circles show
839 relatively oxygenated ones. The full name is placed beside each site. The black dots mark the
840 modeled upwelling regions from Topper et al. (2011), and the gray shading shows areas of
841 prolonged euxinic conditions in the water column given in Jenkyns (2010). HA = High Arctic
842 Large Igneous Province, CP = Caribbean Plateau.

843

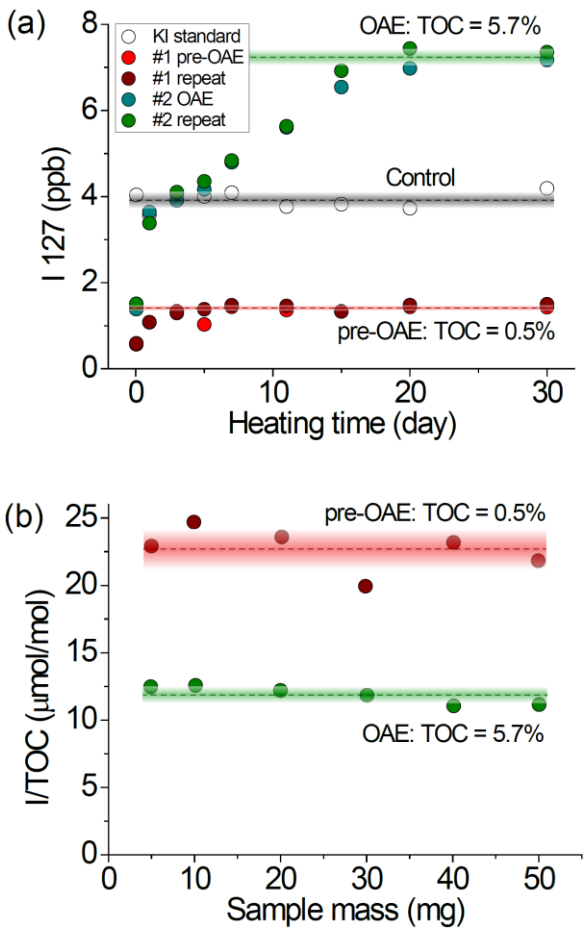

844

845

846 Figure 3. (a). Iodine extraction results of the test run of two OAE 2 samples. Closed circles in red
847 and maroon represent the sample from the pre-OAE interval; closed circles in green and blue are
848 the two identical samples from within the OAE interval; and the open circles denote the KI
849 standard. The plot shows changes in iodine concentration released from the samples with time.
850 The dashed line and colored bars on top of each set of circles are the average value and standard
851 deviation of the data. (b). Effect of sample mass on I/TOC values of the two OAE 2 samples.
852 Legend is the same as figure (a).

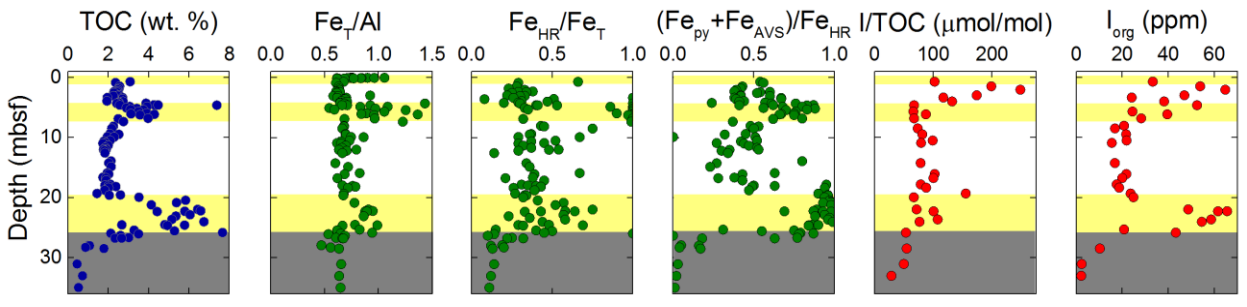

853

854 Figure 4. TOC%, Fe_T/Al, Fe_{HR}/Fe_T, $(Fe_{py}+Fe_{AVS})/Fe_{HR}$, I/TOC, and I_{org} record for the upper 35 m
855 of the Landsort Deep core in the Baltic Sea. Yellow boxes represent euxinic conditions,
856 representing ~2 m, 4.3–7.3 m, and 19.5–26.75 m from the top to the bottom. The gray boxes
857 indicate lacustrine sediments between 25–35 m. TOC% and Fe speciation data are from Hardisty
858 et al. (2016).

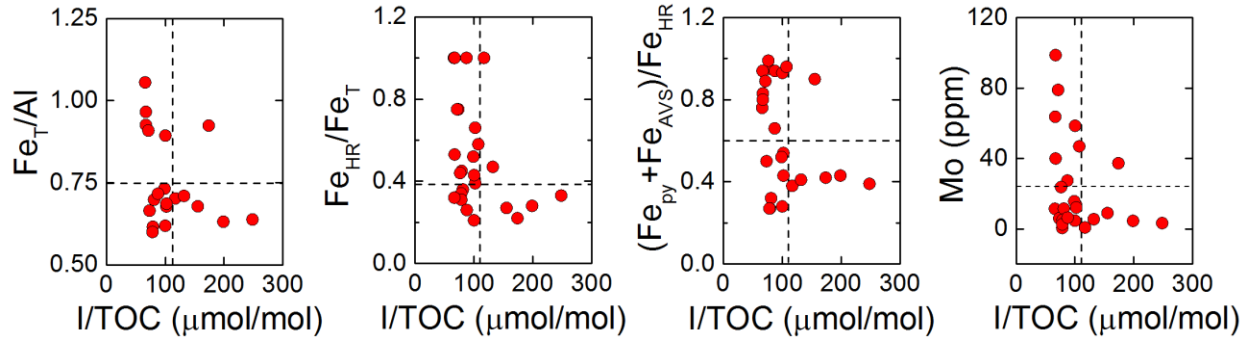

859

860 Figure 5. Fe_T/Al, Fe_{HR}/Fe_T, $(Fe_{py}+Fe_{AVS})/Fe_{HR}$, and Mo concentration plotted against I/TOC
861 through the upper 25 m of the Landsort Deep core in the Baltic Sea. The vertical dashed lines in
862 each plot indicate I/TOC values at 115 μmol/mol, and horizontal lines in each plot represent
863 Fe_T/Al, Fe_{HR}/Fe_T, $(Fe_{py}+Fe_{AVS})/Fe_{HR}$, and Mo concentration of 0.75, 0.38, and 0.6, respectively
864 (Hardisty et al., 2016). Fe_T/Al, Fe_{HR}/Fe_T, $(Fe_{py}+Fe_{AVS})/Fe_{HR}$, Mo concentration above these
865 thresholds suggest euxinic conditions.

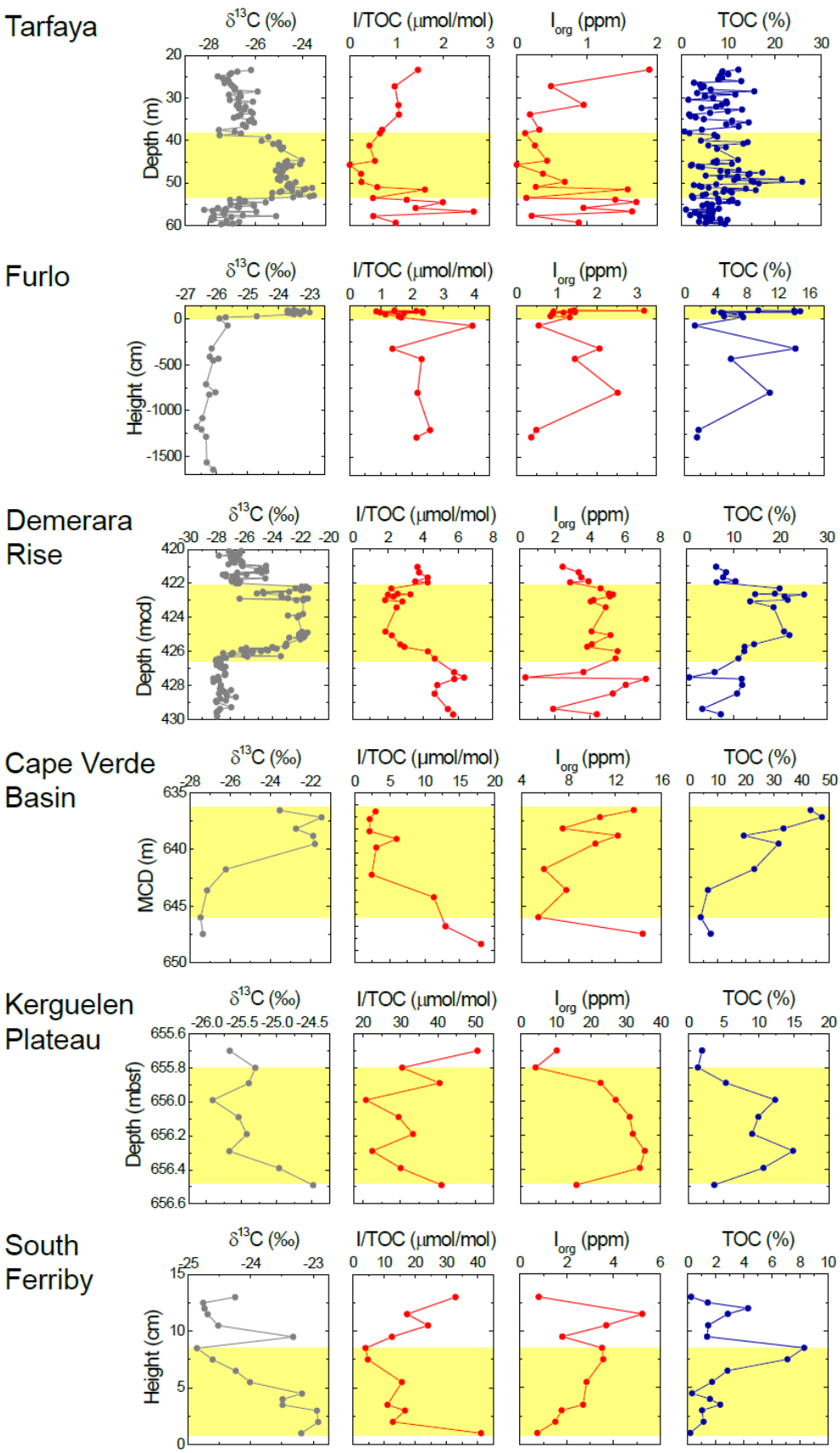
Tarfaya
δ13C (‰)
I/TOC (µmol/mol)
Iorg (ppm)
TOC (%)
Depth (m)
Furlo
Height (cm)
Demerara Rise
Depth (mcd)
Cape Verde Basin
MCD (m)
Kerguelen Plateau
Depth (mbsf)
South Ferriby
Height (cm)

866

867 Figure 6. Stratigraphic records of $\delta^{13}C$, I/TOC, I_{org}, and TOC at the six study sites. I/TOC and I_{org}
868 data are from this study, $\delta^{13}C$ and TOC data are from Holbourn and Kuhnt (2002); Kuypers et al.
869 (2002); Tsikos et al. (2004); Erbacher et al. (2005); and Jenkyns et al. (2007). The yellow boxes
870 bracket the CIE or part of the CIE at each site.

871

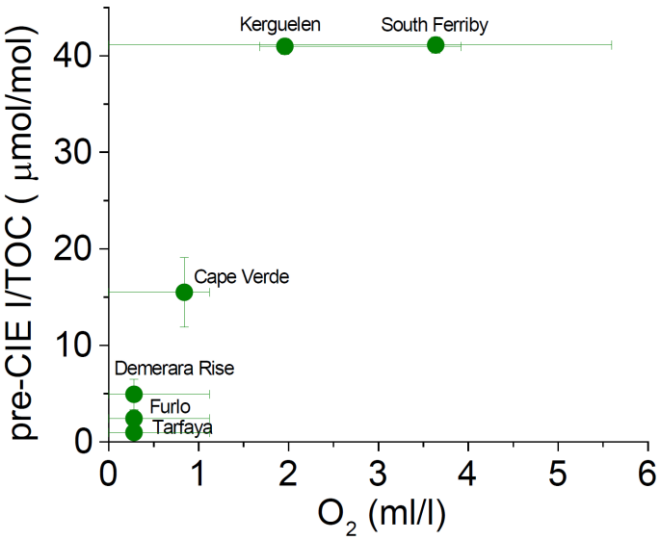

872

873 Figure 7. Pre-CIE average I/TOC values plotted against modeled bottom-water oxygen for the
874 Late Cretaceous with a deeper Panama, after Monteiro et al. (2012). Vertical error bars represent
875 the standard deviation of the average pre-CIE I/TOC value from each site; horizontal error bars
876 are calculated from the surrounding modeled bottom-water O_2 concentrations of each site.

877

878 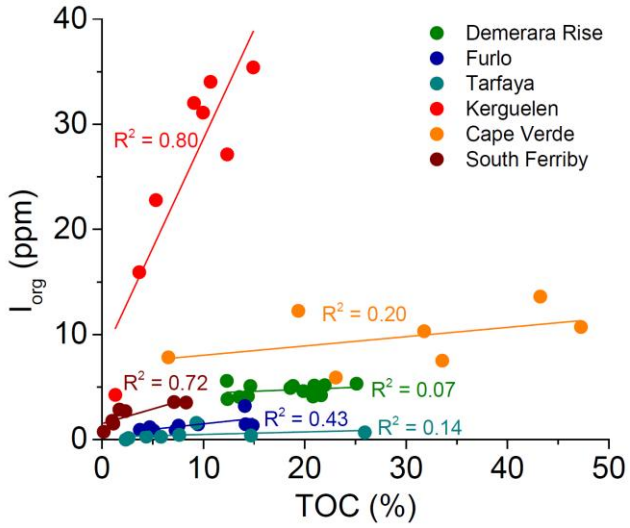

879 Figure 8. Organically bound iodine concentration in bulk sediment (I_{org}) plotted against
880 corresponded TOC content for samples deposited during OAE 2. I_{org} data are from this study;
881 TOC data are from published papers. Circle data points in green, royal blue, dark cyan, red,
882 orange, and maroon colors represent the sites of Demerara Rise, Furlo, Tarfaya, Kerguelen
883 Plateau, Cape Verde Basin, and South Ferriby, respectively. The colored lines across each data
884 set are linear fittings with R^2 indicated in an adjacent position.

885